X-ray induced growth dynamics of luminescent silver clusters in zeolites

Oliver Fenwick, Eduardo Coutiño-Gonzalez,* Fanny Richard, Sara Bonacchi, Wouter Baekelant, Dirk de Vos, Maarten B.J. Roeffaers, Johan Hofkens,* and Paolo Samorì.**

Dr. O. Fenwick, Dr. S. Bonacchi, Dr. F. Richard, Prof. P. Samorì
University of Strasbourg, CNRS, ISIS UMR 7006, 8 Alleé Gaspard Monge, F-67000 Strasbourg, France.
E-mail: samori@unistra.fr

Dr. O. Fenwick
School of Engineering and Materials Science, Queen Mary University of London, Mile End Road, London E1 4NS, United Kingdom.
E-mail: o.fenwick@qmul.ac.uk

Dr. W. Baekelant, Prof. J. Hofkens
Chem&Tech - Molecular Imaging and Photonics, KU Leuven, Celestijnenlaan 200F, B-3001 Leuven, Belgium.
E-mail: johan.hofkens@kuleuven.be

Dr. E. Coutiño-Gonzalez
Centro de Investigaciones en Óptica, A. C. Loma del Bosque 115, Colonia Lomas del Campestre, León, Guanajuato 37150, Mexico.
E-mail: ecoutino@cio.mx

Dr. S. Bonacchi
Dipartimento di Scienze Chimiche, Università di Padova, Via Marzolo, 1. 35131, Padova. Italy.

Prof. Dirk de Vos, Prof. M. B. J. Roeffaers
cMACS, Department of Microbial and Molecular Systems, KU Leuven, Celestijnenlaan 200F, 3001 Heverlee, Belgium.

Abstract

In this work we used $Al_{K\alpha}$ X-rays to drive the growth of luminescent silver clusters in zeolites. We tracked the growth of the silver species using Auger spectroscopy and fluorescence microscopy, by monitoring the evolution from their ions to luminescent clusters and then metallic, dark nanoparticles. We show that the growth rate in different zeolites is determined by the mobility of the silver ions in the framework and that the growth dynamics in calcined samples obeys the Hill-Langmuir equation for non-cooperative binding. Comparison of the optical properties of X-ray grown silver clusters with silver clusters formed by standard heat treatment indicates that the latter have a higher specificity towards the formation of luminescent clusters of a specific (small) nuclearity, whereas the former produces a wide distribution of cluster species as well as larger nanoparticles.

1. Introduction

Small metal clusters with molecular dimensions possess intriguing optical[1] and catalytic[2] properties that are not observed in bulk metals. Being able to tune these properties by fine control of the cluster nuclearity and geometry has been the focus of much research. Nonetheless, precise control of the cluster size remains challenging due to their tendency to aggregate into larger particles exhibiting bulk properties. Consequently, a number of approaches have been proposed to stabilize clusters of various sizes, including molecular approaches based on DNA,[1, 3] polymers[4-6] and peptides,[7] and inorganic approaches relying on glasses[8-9] and zeolites.[10-15] We have recently reported luminescence of silver clusters in calcined zeolites, with photoluminescence quantum efficiencies nearing 100 % when the interaction between the silver atoms and the host is optimised.[10] This makes zeolites particularly attractive hosts for the stabilization of luminescent silver clusters and other metals for applications in lighting,[16] as luminescent tags,[17] as humidity sensors,[18-19] and for biological imaging.[20-22]

Zeolites are porous materials comprising a negatively-charged aluminosilicate framework balanced by extra-framework cations in the pores. These cations are usually alkaline or alkaline-earth metal ions, but can be readily exchanged with metal or organic cations.[22-24] The nature of the clusters that can be formed from these ion-exchanged starting materials depends on the interaction of the cation(s) with the matrix, which in the case of zeolites is determined primarily by the topology of the framework, the framework charge, cation type and interaction with other extra-framework cations. The formation of metal clusters from extra-framework cations requires an extra stimulus which can be provided by UV photon irradiation,[17, 25-26] thermal treatment,[10, 26-27] solid-gas reactions,[28] electron beams[29] or X-rays.[30-32] Whilst the determination of the exact nature of the metal clusters has been the focus of several recent studies,[10, 33-35] the dynamics of small cluster formation and growth is significantly less well studied. A previous

attempt using the electron beam of a TEM[29] revealed the evolution of nm-sized metallic Ag clusters (~50-100 atoms) in zeolite pores to larger nanoparticles on the surface. Our own prior attempt using XANES was also unable to study the early stage of cluster formation due to poor time resolution[30] though *in situ* point distribution functions has been shown to yield some results for clusters formed by solid-gas reactions.[28] In a separate work, we were able to follow the development of photoluminescence when activating cluster formation using UV light, though this did not reveal the physical structure of the clusters.[25] If we are to fully harness the properties of metal clusters then we must address this knowledge deficit.

In this paper, we study the formation of silver clusters in four different Ag-faujasite samples under X-ray irradiation inside an X-ray photoelectron spectrometer. The framework structure (faujasite, FAU) of the zeolites studied is identical, but tuning the chemical composition (i.e. the Si/Al ratio and hence the degree of cation exchange capacity) allowed us to study the influence of the local environment experienced by the extra-framework cations on the rate of silver cluster growth. We monitored the formation of silver species as a function of X-ray dose whilst characterizing them *in-situ* using Auger spectroscopy and *ex-situ* by fluorescence imaging. We observe the formation of luminescent silver clusters and their growth into larger clusters and ultimately into metallic nanoparticles, and propose a model for the dynamics.

2. Results and Discussion

Starting from the parent FAU zeolites (**Fig. 1a**) in their sodium form, silver exchange was carried out in an aqueous silver nitrate solution. Note that depending on the composition – the SiO_2/Al_2O_3 ratio - synthetic FAU zeolites are named X, FAUX, with $2 > SiO_2/Al_2O_3 > 3$ and Y, FAUY, with $SiO_2/Al_2O_3 > 3$. We obtained fully- and partially-exchanged zeolites, which we refer to according to their nominal silver content relative to the dehydrated unit cells normalised

to 24 T-atoms (the tetrahedrally coordinated Si and Al atoms). These are: $(Ag^{+}_{x}Na^{+}_{11-x})[Al_{11}Si_{13}O_{48}]$, referred to as FAUX[$Ag_x$], and $(Ag^{+}_{x}Na^{+}_{6.5-x})[Al_{6.5}Si_{17.5}O_{48}]$, referred to as FAUY[$Ag_x$]. We chose FAUX[$Ag_6$], FAUX[$Ag_{11}$], FAUY[$Ag_3$] and FAUY[$Ag_{6.5}$] zeolites for this study due to our previous observation[10] of high photoluminescence in Ag-faujasite systems, which is highly dependent on the degree of silver exchange and the Si/Al ratio of the framework. We note that the FAUX[Ag_{11}] and FAUY[$Ag_{6.5}$] zeolites are fully ion exchanged. Materials were studied in their cation-exchanged form (dried at 100 °C after ion exchange without thermal activation at elevated temperatures), or, where indicated in the text, in their calcined form (thermally activated at 450 °C in air to allow cluster formation, prior to other measurements).

X-ray irradiation of the samples was performed by using the AlK_α source (h ν = 1486.7 eV) of a Thermo Scientific™ K-Alpha™ X-ray Photoelectron Spectrometer (XPS) system, with the X-rays focussed to a 200 μm spot (power density = 66 W/m^2). Variable X-ray doses could be applied to the surface of the sample with a minimum single dose of 0.9 kJ/m^2. Silver Auger spectra were measured during X-ray exposure. The minimum dose required to obtain an Auger spectrum with its partner $3d_{5/2}$ spectrum of sufficiently high signal to noise ratio to calculate an Auger parameter was 8 kJ/m^2 (120s acquisition time). To obtain Auger spectra of sufficient quality for accurate peak fitting the minimum X-ray dose was 16 kJ/m^2 (240 s acquisition time). An electron flood gun was applied during the XPS measurements to minimize charging effects. The X-rays themselves penetrate into the bulk of the zeolite crystals, triggering silver cluster growth throughout. However, the significantly lower mean free path of photoelectrons means that the information in XPS and Auger spectra only comes from a surface layer ~10 nm thick.

The Auger spectrum of silver ions and clusters exhibit two broad bands with kinetic energies near 348 eV (Ag $M_5N_{45}N_{45}$) and 353 eV[10] (Ag $M_4N_{45}N_{45}$) visible in the spectra of the cation-exchanged zeolites (**Fig. 1b**) and their calcined analogues.[10] These are distinct from the characteristic spectrum of metallic silver which can be described by the superposition of 6 individual peaks,[10, 36-38] and can be observed for nanoparticles with diameter ≥10 nm.[10]

In our first experiment we recorded multiple Auger spectra with long acquisition times (≥120 seconds at 66 W/m^2) focussed at the same location on the Ag-zeolite powders. The initial Auger spectra showed the clear two-band signature of silver ions (or clusters) with peaks at 348 and 353 eV, but subsequent spectra show the gradual emergence of the metallic signature which we take as an indication of silver agglomeration to form nanoparticles of increasing size (**Fig. 1b**). The full Auger spectra were fitted and the evolution of the main metallic peaks plotted in Figure S4 (Supporting Information). This trend was observed in all of our Ag-zeolite powders, but distinct differences in the rate of appearance of the metallic peaks is evident in Figure S4. In fact, the FAUY zeolites have small metallic peaks even in the first Auger spectrum.

We defined the Auger spectrum as being metallic or not by calculating the modified Auger parameter of each zeolite as a function of the X-ray dose (**Fig. 1c**). The modified Auger parameter is a quantitative measure of the shift in atomic orbital energy due to their chemical environment (bonding, oxidation state, among others) and it is equal to the sum of the binding energy of $3d_{5/2}$ electrons and the kinetic energy of $M_4N_{4,5}N_{4,5}$ Auger electrons. It has the benefit of being particularly sensitive to chemical state (since Auger emission is a three-electron process), and it is also immune to shifts caused by sample charging during the measurement.[39] The modified Auger parameter for metallic silver is widely reported in the range 726.0 eV to 726.5 eV.[10, 36-37, 40] On the other hand, the modified Auger parameters of silver ions, salts and clusters are lower than metallic silver by up to 4 eV.[36] Previous studies have reported modified

Auger parameters of silver species in calcined FAU and LTA zeolites of 722 - 724 eV,[10, 41] whilst there are differing values of ~722 eV[42] and ~726 eV[41] (metallic) reported for silver species in mordenite. In our cation-exchanged (non-calcined) zeolites after the minimum X-ray exposure, we measure modified Auger parameters of 722.4 eV (FAUX[Ag_6]), 722.9 eV (FAUX[Ag_{11}]), 722.5 eV (FAUY[Ag_3]) and 722.0 eV (FAUY[$Ag_{6.5}$]), which are similar to values for the calcined versions of these zeolites published in our previous work.[10]

We tracked the modified Auger parameter as a function of the X-ray dose (**Fig. 1c**), finding that the modified Auger parameter switches from the ion/cluster value (722-723 eV) to the metallic value (~726 eV) at a critical X-ray dose. This critical dose, does not represent a sudden change in the cluster structure, rather the characteristic metallic peak in the spectrum grows gradually (Figure S4, Supporting Information) and finally becomes larger than the other $M_4N_{4,5}N_{4,5}$ Auger peak after this "critical" X-ray dose. We used this "critical" dose as a measure of the resilience of silver species against X-rays in each of the four samples (Errore. L'origine riferimento non è stata trovata., **Fig. 1d**). The higher the dose that can be absorbed before the metallic signature dominates, the more stable the silver ions/clusters are. Our results clearly show two trends: (i) silver clusters in FAUX zeolites are more stable to X-ray exposure than clusters in FAUY; and (ii) when the zeolite is fully exchanged with silver ions, they are more stable to X-ray exposure than when partially exchanged.

At first sight, these trends may seem counterintuitive, since (i) FAUX and FAUY zeolites have identical topology; and (ii) in highly loaded silver zeolites, the average silver-silver interatom distance is smaller which one might expect to accelerate agglomeration. In fact, the mobility of extra-framework cations in zeolites is a complex trade-off between the framework-cation interaction, and cation-cation repulsion. Polarizability can also play a significant role in hydrated systems,[43] though we consider our zeolites to be largely dehydrated due to the thermal

treatment after ion exchange (100 °C for 1 hour) and even more so due to the high vacuum environment of the XPS chamber. We have previously shown that weight loss in LTA zeolites due to water desorption starts at 50°C,[19] and thermogravimetric analysis indicates a similar temperature threshold for dehydration in our FAU zeolites (see Supporting Information, Figure S3). The Coulombic energy of the framework-cation interaction (F_{el}) is a function of the cation radius, r_+, and the effective (framework) anion radius, r_-:.[43-44]

$$F_{el} \propto -1/(r_+ + r_-) \quad (1)$$

To account for the anionic field strength in the framework, r_- is larger when the framework charge density is lower (i.e. when the Si/Al ratio is larger). Therefore, $|F_{el}|$ is larger for Na^+ cations than for Ag^+ ($|F_{el}|_{Na} > |F_{el}|_{Ag}$), and is larger in FAUX frameworks than FAUY ($|F_{el}|_{FAUX} > |F_{el}|_{FAUY}$). Cation-cation repulsion increases with ionic radius and with the density of ions[45] and can therefore be significant at high loading of Ag^+ ions and is more significant in FAUX than FAUY due to the higher capacity for cations in FAUX (i.e. the higher framework charge density). As the silver loading is increased in either framework, it is the cation-cation repulsion which lowers Ag^+ mobility and stabilises our silver species. Interestingly, it has been reported that Na^+ ions are more mobile than Ag^+ ions in FAUX, but the opposite is true for FAUY.[46-48] Since $|F_{el}|_{Na} > |F_{el}|_{Ag}$ in both frameworks, we can consider this a result of more significant cation-cation repulsion limiting Ag^+ mobility in FAUX. In our previous work,[10] we correlated the exceptional photoluminescence efficiency of silver clusters in FAUY zeolites (at low levels of silver exchange) to a high degree of order within clusters enabled by a high mobility of Ag^+ compared to Na^+. In FAUX zeolites, where Na^+ cation mobility is higher than Ag^+, we detected a sodium shell around the silver clusters (absent in FAUY) that was interfering in cluster formation. To summarise results of the current work, silver-exchanged FAUX zeolites require a larger X-ray dose to develop metallic silver characteristics than the FAUY zeolites, which we link to the larger $|F_{el}|$ in FAUX, a larger cation-cation repulsion in FAUX and a competitive role of Na^+ interfering with cluster growth in FAUX. The resilience to X-ray

induced cluster growth at higher degrees of silver loading in both frameworks can be linked to an increase in cation-cation repulsion that reduces the Ag^+ mobility.

To further investigate the nature of the silver species formed by X-ray irradiation, we irradiated FAUX[Ag_{11}] samples with short X-ray doses (minimum dose 0.9 kJ/m^2) then transferred them to a light microscope, where we imaged them in bright-field and in fluorescence mode with excitation wavelengths of 312, 365 and 475 nm. In our previous work we showed that upon calcination of silver-exchanged FAU zeolites, highly luminescent silver clusters form inside the sodalite cages.[10] These clusters with nuclearity of 4 have an absorption peak that is well matched to 312 nm excitation, but the absorbance is much reduced at 365 nm (**Fig. 2**). The long wavelength excitation sources (365 m, and 475 nm) are chosen to probe larger clusters and nanoparticles which may develop after prolonged X-ray exposure. Mie and Drude theories predict increasing photoabsorption peak wavelength for increasing nanoparticle diameter,[49] whilst molecular-sized silver clusters also show a narrowing of their HOMO-LUMO gap with increasing cluster size (though the trend is not quite monotonic).[49-51] In a recent work we did observe high nuclearity (Ag_6) metal clusters whose absorption peaks at 560 nm (with weak absorption at our longest excitation wavelength, 475 nm).[52]

Fluorescence images obtained with 312 nm excitation and collection in the range 520 – 1100 nm show that low X-ray doses ($\leq$ 3 kJ/m^2) cause a feeble yellow luminescence to develop in the X-ray irradiated zone, consistent with the formation of small Ag_4 clusters (**Fig. 3a,b**). We note that vacuum alone has been reported to induce cluster formation[13] and luminesce[34] in Ag-zeolites. However, it is clear from our images that the luminescence only develops in areas exposed to the X-ray beam, so we consider the X-rays to be the main driver for cluster formation on the timescale of our experiment. Continued irradiation leads to a quenching of this luminescence. The intensity of the luminescence in the central irradiated area is plotted as a

function of X-ray dose in **Fig. 3b**. A similar set of images obtained with 365 nm excitation show a similar trend, but the peak in luminescence occurs at larger X-ray doses (~5 kJ/m^2) before decaying at approximately the same rate as the 312 nm excitation case. For 475 nm excitation the peak luminescence is even further shifted to large X-ray doses (>10 kJ/m^2). Since excitation by different wavelengths of light enables us to probe clusters of different sizes, the observation of peak luminescence occurring after larger X-ray doses for longer wavelength excitation is therefore consistent with X-ray induced agglomeration of silver ions to form progressively larger clusters. Although the light does not penetrate through the full thickness of the zeolite particles, it should penetrate to depths of 100 nm or more so probes a mixture of the surface and subsurface silver clusters.

At the highest X-ray doses, photoluminescence of the silver species cannot be excited by our longest excitation wavelength (475 nm) - the particles have become too large (and too metallic) to show luminescence. The emergence of a metallic phase is suggested by the bright field image, which reveals dark particles developing in the irradiated area (visible above 20 kJ/m^2 doses). This is confirmed by the emergence of a metallic signature in the Auger spectra after long X-ray exposure (**Fig. 1b**). The metallic signature allows us to rule out mixed oxide species within the framework as being the source of the dark particles in the bright-field image; an effect that has previously been reported for X-ray irradiation of FAU-zeolites containing multivalent cations.[53] We note that, as well as on the surface, it is possible that spherical nanoparticles of up to ~11 Å diameter could form inside the zeolite pore, although these are not visible optically. Since the drop in photoluminescence signal occurs at lower X-ray doses than needed for the metallic components of the Auger spectra to dominate (>200 kJ/m^2 in FAUX), it is likely that much of the initial drop in photoluminescence occurs predominantly due to large cluster formation with further red-shifted absorption or low emission efficiencies.[10]

To better understand the mechanism of cluster formation we also investigated the evolution of photoluminescence in calcined analogues of the same zeolites (**Fig. 4a,b**). Our starting point in this case is known to be luminescent Ag_4 clusters[10] with the excitation-emission spectra depicted in **Fig. 2**. We also note that the calcination treatment at 450 °C completely dehydrates the system (19-20 % weight loss, Fig. S3). Using excitation which matches the absorption of these clusters (312 nm) we see a progressive decrease in photoluminescence signal which starts after an initial delay (**Fig. 4a**). This is mimicked precisely using excitation at 365 nm, which has a small overlap with the absorption of these clusters (**Fig. 2**). The evolution of the photoluminescence (PL) follows a specific sigmoidal function:

$$PL = PL_0 \cdot \frac{K^n}{K^n + D^n} \qquad (2)$$

This is a form of the Hill-Langmuir equation where *PL* and PL_0 are the photoluminescence (PL) and initial PL signal respectively. In the case of the bright-field images we use brightness and initial brightness of the image instead of photoluminescence signal. D is the X-ray dose in kJ/m^2, *K* is a constant and in the Hill-Langmuir model it is related to the activation energies of adsorption and desorption along with the concentration of binding sites. For the calcined FAUX[Ag_{11}] (**Fig. 4c**), we find *K* to be dependent on the excitation source, with $K_{312\ nm}$=$K_{365\ nm}$ < $K_{Bright\ field}$ (72 ± 8, 72 ± 6, and 361 ± 31 kJ/m^2, respectively). The similarity between $K_{312\ nm}$ and $K_{365\ nm}$ is reassuring, since both wavelengths probe similar sized clusters. The larger value for $K_{Bright\ field}$ tells us that there is a greater activation energy associated with forming large metallic clusters compared to small UV absorbing clusters or that the number of possible binding sites is reduced. The constant *n* gives an indication of cooperativity in the binding process where $n < 1$ implies negatively cooperative binding, whilst $n > 1$ implies positively cooperative binding. Importantly, for our data we find $n = 1$. This is interesting since it implies that the growth kinetics of the clusters proceeds in the same manner as a gas of atoms binding

non-cooperatively to a fixed number of zeolite framework sites. Whereas thermal treatment may not be able to activate larger cluster formation (i.e. the nuclearity stabilises at 4), energetic barriers to large cluster formation are small compared to the X-ray photon energy (1486.7 eV) and growth in this case is unlimited.

Under 475 nm illumination, which is not absorbed by Ag_4 clusters, the calcined zeolites show behaviour reminiscent of the cation-exchanged zeolites which had not been heat-activated prior to X-ray irradiation, i.e. an initial increase in photoluminescence signal corresponding to the development of Ag clusters of a certain size that can be probed by the 475 nm excitation ($n > 4$) followed by a decrease as the silver particles grow even larger.

The correlation between the photoluminescence decrease of the calcined zeolite under 312 nm and 365 nm excitation was not replicated in the cation-exchanged zeolites which had not been heat activated (**Fig. 3b**). In that case, the rise and fall of the photoluminescence signal was retarded under 365 nm illumination compared to 312 nm illumination. This confirms our previous observation[10] of the remarkable homogeneity of the silver clusters in the heat-activated Ag-FAU zeolites, but also tells us that this homogeneity is not replicated when the silver clusters are grown under X-ray irradiation where we have a mixture of cluster sizes (and locations) at all stages of the growth process.

3. Conclusion

In summary we have monitored the X-ray induced growth of silver clusters in zeolites by *in-situ* monitoring of the silver Auger spectra and also by *ex-situ* recording of the photoluminescence. We have observed the growth of silver species from ions to metallic nanoparticles, and can obtain luminescent clusters from intermediate X-ray doses. We found

that the growth rate (R) of silver species differs in the four FAU zeolites studied, following the trend $R_{FAUY[Ag_3]} > R_{FAUY[Ag_{6.5}]} > R_{FAUX[Ag_6]} > R_{FAUX[Ag_{11}]}$. This trend correlates with the silver ion mobility, M, in the zeolite frameworks, where $M_{FAUY} > M_{FAUX}$ and M is lower when the degree of silver exchange is higher. The growth and subsequent decay in the photoluminescence signal under progressively increasing X-ray dose was found to be a good proxy for the growth dynamics of species of different sizes due to the longer absorption wavelength of larger species. We demonstrated that the growth of silver species follows a non-cooperative Hill-Langmuir type behaviour. Furthermore, we found that silver clusters formed in zeolites by X-ray irradiation may have a more disperse size distribution than silver clusters formed in zeolites by thermal calcination. Our insight into the stability of silver clusters in zeolites and their growth dynamics is an important addition to our understanding of these systems whose luminescent and catalytic properties are attracting increasing attention for a number of applications. Moreover, these findings could be applicable for other metal clusters and nanoparticles in zeolites or analogous porous frameworks.

4. Experimental Section

Sample preparation: In this study, FAU zeolites (FAUX, Si/Al ratio 1.2 from UOP, and FAUY Si/Al ratio 2.7 from ZEOLYST) were used. A cation exchange procedure was employed to generate the silver exchanged FAU zeolites. In brief, one gram of zeolite material was suspended in 500 mL of an aqueous silver nitrate solution ($AgNO_3$ Sigma-Aldrich, 99.99% purity) with the desired concentration to achieve different silver loadings. The sample was left overnight in an end-over-end shaker for agitation in the dark. The samples were recovered by filtration using a Büchner filter and washed several times with deionized water. The recovered powder was dried at 100 °C for 1 hour (cation-exchanged samples), to remove the excess water;

and for the case of calcined samples a heat-treatment at 450 °C (overnight), using a temperature ramp of 5 °C /min, was carried on a muffle.

X-ray photoelectron spectroscopy (XPS): X-ray exposure of the samples in powder form was achieved using a Thermo Scientific™ K-Alpha™ X-ray Photoelectron Spectrometer (XPS) system. The AlK_{α} source produces x-rays (*hv = 1486.7 eV)* that are focussed to a 200 μm spot (power density = 66 W/m^2). X-ray doses could be applied to the surface of the sample in doses as small as 1 kJ/m^2. $Ag3d_{5/2}$ spectra and Ag Auger spectra were measured simultaneously during X-ray exposure with a pass-energy of 50 eV and step of 0.1 eV. An electron flood gun was applied during the XPS measurements to minimize charging effects.

Fluorescence microscopy: After X-ray exposure the samples were imaged with an Olympus BX51 TRF fluorescence microscope coupled with an Olympus DP-73 camera. Excitation was provided either by a UV lamp (312 nm and 365 nm) or by a broadband source (20 W Hg vapor lamp - Lumen Dynamics X-Cite 120Q) combined with a filter cube (U-MWBS3; excitation band-pass filter 460-490 nm, emission cut-on filter 520 nm, dichromatic mirror 500 nm). For each series of zeolite powder samples (i.e. a series of measurements relating to one starting zeolite material with multiple X-ray exposures), the illumination and detection parameters were kept constant (lamp power, acquisition time, ISO, and number of averages), enabling quantitative comparison of the recorded intensities.

Supporting Information

Supporting Information is available from the Wiley Online Library or from the author.

Acknowledgements

This work was financially supported by EC through the projects FP7-NMP-2012 SACS (GA-310651), the ERC projects SUPRAFUNCTION (GA-257305), LIGHT (GA-307523) and FLUOROCODE (GA-291593), the Marie-Curie project IEF-MULTITUDES (PIEF-GA-2012-326666), the Agence Nationale de la Recherche through the LabEx project Chemistry of Complex Systems (ANR-10-LABX-0026_CSC), the International Center for Frontier Research in Chemistry (icFRC), the 'Fonds voor Wetenschappelijk Onderzoek FWO' (G.0962.13, ZW15_09GOH6316, 12Y6418N and G.098319N), the Flemish government (long term structural funding-Methusalem grant CASAS2, Meth/15/04), the KU Leuven Research Fund (C14/15/053), the Hercules foundation (HER/11/14), and the Belgian Federal Science Policy Office (IAP-VII/05). OF acknowledges the support of the Royal Society through a University Research Fellowship (URF140372). ECG acknowledges the support provided by CONACYT through the project A1-S-44458 (Ciencia Básica funds). We would like to thank UOP Antwerpen for their donation of the zeolites.

Received: ((will be filled in by the editorial staff))
Revised: ((will be filled in by the editorial staff))
Published online: ((will be filled in by the editorial staff))

Conflict of Interest

The authors declare no conflict of interest.

Keywords

Zeolite, silver clusters, luminescence, XPS analysis, growth dynamics, Hill-Langmuir equation for non-cooperative binding.

References

1. T. Vosch, Y. Antoku, J.C. Hsiang, C.I. Richards, J.I. Gonzalez, R.M. Dickson, *Proc. Natl. Acad. Sci. USA* **2007,** *104*, 12616.

2. J.A. Martens, A. Cauvel, A. Francis, C. Hermans, F. Jayat, M. Remy, M. Keung, J. Lievens, P.A. Jacobs, *Angew. Chem. Int. Ed.* **1998,** *37*, 1901.

3. C.I. Richards, S. Choi, J.C. Hsiang, Y. Antoku, T. Vosch, A. Bongiorno, Y. Tzeng, R.M. Dickson, *J. Am. Chem. Soc.* **2008,** *130*, 5038.

4. A. Henglein, *Chem. Rev.* **1989,** *89*, 1861.

5. P. Mulvaney, A. Henglein, *J. Phys. Chem.* **1990,** *94*, 4182.

6. I. Diez, M.I. Kanyuk, A.P. Demchenko, A. Walther, H. Jiang, O. Ikkala, R.H.A. Ras, *Nanoscale* **2012,** *4*, 4434.

7. J. Yu, S.A. Patel, R.M. Dickson, *Angew. Chem.* **2007,** *119*, 2074.

8. E. Borsella, E. Cattaruzza, G. De Marchi, F. Gonella, G. Mattei, P. Mazzoldi, A. Quaranta, G. Battaglin, R. Polloni, *J. Non-Crys. Sol.* **1999,** *245*, 122.

9. M.V. Shestakov, X. Chen, W. Baekelant, A.S. Kuznetsov, V.K. Tikhomirov, J. Hofkens, V.V. Moshchalkov, *RSC Adv.* **2014,** *4*, 20699.

10. O. Fenwick, E. Coutino-Gonzalez, D. Grandjean, W. Baekelant, F. Richard, S. Bonacchi, D. De Vos, P. Lievens, M. Roeffaers, J. Hofkens, P. Samori, *Nat. Mater.* **2016,** *15*, 1017.

11. E. Coutino-Gonzalez, M.B.J. Roeffaers, B. Dieu, G. De Cremer, S. Leyre, P. Hanselaer, W. Fyen, B. Sels, J. Hofkens, *J. Phys. Chem. C* **2013,** *117*, 6998.

12. P.J. Grobet, R.A. Schoonheydt, *Surf. Sci.* **1985,** *156*, 893.

13. R. Seifert, A. Kunzmann, G. Calzaferri, *Angew. Chem. Int. Ed.* **1998,** *37*, 1521.

14. T. Wasowicz, J. Michalik, *Rad. Phys. & Chem.* **1991,** *37*, 427.

15. B. Dong, R. Retoux, V. de Waele, S.G. Chiodo, T. Mineva, J. Cardin, S. Mintova, *Microporous Mesoporous Mat.* **2017,** *244*, 74.

16. W. Baekelant, S. Aghakhani, E. Fron, C. Martin, C. Woong-Kim, J.A. Steele, T. De Baerdemaeker, F. D´Acapito, D. Chernysov, M. van der Auweraer, P. Lievens, D. Grandejan, M.B.J. Roeffaers, J. Hofkens, E. Coutiño.Gonzalez, *J. Mater. Chem. C* **2019,** *7*, 14366.

17. G. De Cremer, B.F. Sels, J. Hotta, M.B.J. Roeffaers, E. Bartholomeeusen, E. Coutino-Gonzalez, V. Valtchev, D.E. De Vos, T. Vosch, J. Hofkens, *Adv. Mater.* **2010,** *22*, 957.

18. E. Coutino-Gonzalez, W. Baekelant, B. Dieu, M.B.J. Roeffaers, J. Hofkens, *J. Vis. Exp.* **2016,** *117*, 54674.

19. E. Coutino-Gonzalez, W. Baekelant, D. Grandjean, M.B.J. Roeffaers, E. Fron, M.S. Aghakhani, N. Bovet, M. Van der Auweraer, P. Lievens, T. Vosch, B. Sels, J. Hofkens, *J. Mater. Chem. C* **2015,** *3*, 11857.

20. H. Awala, J.-P. Gilson, R. Retoux, P. Boullay, J.-M. Goupil, V. Valtchev, S. Mintova, *Nat. Mater.* **2015,** *14*, 447.

21. G. De Cremer, E. Coutino-Gonzalez, M.B.J. Roeffaers, B. Moens, J. Ollevier, M. Van der Auweraer, R. Schoonheydt, P.A. Jacobs, F.C. De Schryver, J. Hofkens, D.E. De Vos, B.F. Sels, T. Vosch, *J. Am. Chem. Soc.* **2009,** *131*, 3049.

22. M. Busby, A. Devaux, C. Blum, V. Subramaniam, G. Calzaferri, L. De Cola, *J. Phys. Chem. C* **2011,** *115*, 5974.

23. C. Leiggener, G. Calzaferri, *Chem. Eur. J.* **2005,** *11*, 7191.

24. P. Cao, O. Khorev, A. Devaux, L. Sägesser, A. Kunzmann, A. Ecker, R. Häner, D. Brühwiler, G. Calzaferri, P. Belser, *Chem. Eur. J.* **2016,** *22*, 4046.

25. G. De Cremer, Y. Antoku, M.B.J. Roeffaers, M. Sliwa, J. Van Noyen, S. Smout, J. Hofkens, D.E. De Vos, B.F. Sels, T. Vosch, *Angew. Chem. Int. Ed.* **2008,** *47*, 2813.

26. K. Bourhis, A. Royon, G. Papon, M. Bellec, Y. Petit, L. Canioni, M. Dussauze, V. Rodriguez, L. Binet, D. Caurant, M. Treguer, J.-J. Videau, T. Cardinal, *Mater. Res. Bull.* **2013,** *48*, 1637.

27. W. Baekelant, G. Romolini, L. Sun, M. De Ras, E. Fron, T. Moreira, C. Viola, A. Ruivo, C.A.T. Laia, J. Maartens, C. Martin, C Woong-Kim, M. van der Auweraer, M.B.J. Roeffaers, J. Hofkens, E. Coutino-Gonzalez, *Methods Appl. Fluoresc.* **2020,** *8*, 024004.

28. H. Zhao, T.M. Nenoff, G. Jennings, P.J. Chupas, K.W. Chapman, *J. Phys. Chem. Lett.* **2011,** *2*, 2742.

29. Y. Sasaki, T. Suzuki, *Mater. Trans.* **2009,** *50*, 1050.

30. E. Coutino-Gonzalez, D. Grandjean, M.B.J. Roeffaers, K. Kvashnina, E. Fron, B. Dieu, G. De Cremer, P. Lievens, B. Sels, J. Hofkens, *Chem. Commun.* **2014,** *50*, 1350.

31. E. Maik, R. Klaus, H. Armin, M.T. Dragomir, W. Wilfried, S. Reinhard, P. Gianfranco, *Nanotechnology* **2008,** *19*, 135701.

32. K. Taiji, Y. Iso, T. Isobe, *J. Lumin.* **2018,** *196*, 214.

33. D. Grandjean, E. Coutiño-Gonzalez, N.T. Cuong, E. Fron, W. Baekelant, S. Aghakhani, P. Schlexer, F. D'Acapito, D. Banerjee, M.B.J. Roeffaers, M.T. Nguyen, J. Hofkens, P. Lievens, *Science* **2018,** *361*, 686.

34. T. Altantzis, E. Coutino-Gonzalez, W. Baekelant, G.T. Martinez, A.M. Abakumov, G.V.Tendeloo, M.B.J. Roeffaers, S. Bals, J. Hofkens, *ACS Nano* **2016,** *10*, 7604.

35. T. Miyanaga, Y. Suzuki, N. Matsumoto, S. Narita, T. Ainai, H. Hoshino, *Microporous Mesoporous Mat.* **2013,** *168*, 213.

36. A.M. Ferraria, A.P. Carapeto, A.M. Botelho do Rego, *Vacuum* **2012,** *86*, 1988.

37. V.K. Kaushik, *J. Elect. Spectros. & Relat. Phenomena* **1991,** *56*, 273.

38. P.J. Bassett, T.E. Gallon, J.A.D. Matthew, M. Prutton, *Surf. Sci.* **1973,** *35*, 63.

39. S.W. Gaarenstroom, N. Winograd, *J. Chem. Phys.* **1977,** *67*, 3500.

40. C.D. Wagner, L.H. Gale, R.H. Raymond, *Analyt. Chem.* **1979,** *51*, 466.

41. A.M. Fonseca, I.C. Neves, *Microporous Mesoporous Mat.* **2013,** *181*, 83.

42. S.G. Aspromonte, M.D. Mizrahi, F.A. Schneeberger, J.M.R. López, A.V. Boix, *J. Phys. Chem. C* **2013,** *117*, 25433.

43. J.A. Marinsky, The ion-exchange properties of zeolites. In *Ion Exchange*, J.A. Marinsky, Ed. Marcel Dekker, Inc.: New York, 1969; Vol. 2, pp 89-133.

44. G. Eisenman, *Biophys. J.* **1962,** *2*, 259.

45. I.M. Kalogeras, A. Vassilikou-Dova, *Defect & Diff. Forum* **1998,** *164*, 1-36.

46. D.C. Freeman, D.N. Stamires, *J. Chem. Phys.* **1961,** *35*, 799.

47. W.J. Mortier, R.A. Schoonheydt, *Prog. Sol. State Chem.* **1985,** *16*, 1.

48. U. Simon, M.E. Franke, *Microporous Mesoporous Mat.* **2000,** *41*, 1.

49. W.A. de Heer, *Rev. Mod. Phys.* **1993,** *65*, 611.

50. C. Jackschath, I. Rabin, W. Schulze, *Zeitschrift für Physik D Atoms, Molecules and Clusters* **1992,** *22* , 517.

51. G. Alameddin, J. Hunter, D. Cameron, M.M. Kappes, *Chem. Phys. Lett.* **1992,** *192*, 122.

52. S. Aghakhani, D. Grandjean, W. Baekelant, E. Coutiño-Gonzalez, E. Fron, K. Kvashnina, M.B.J. Roeffaers, J. Hofkens, B.F. Sels, P. Lievens, *Nanoscale* **2018,** *10*, 11467.

53. M.L. Costenoble, W.J. Mortier, J.B. Uytterhoeven, *J. Chem. Soc. Faraday Trans.* **1978,** *74*, 477.

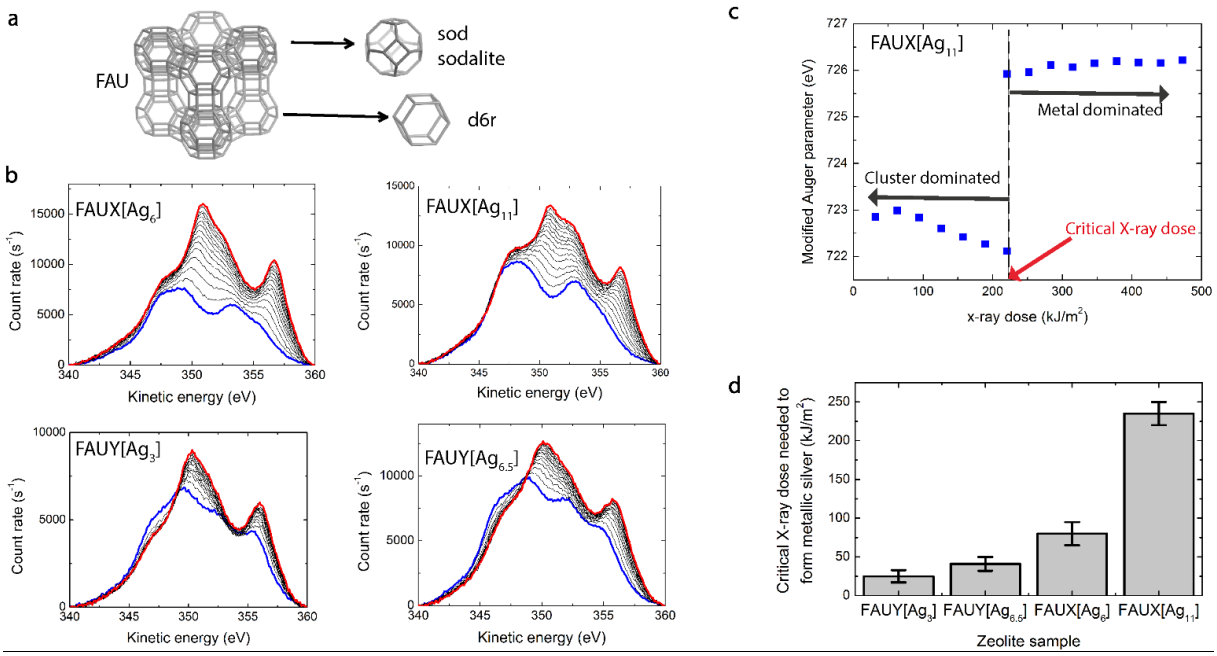

Figure 1. (a) Topology of faujasite (FAU) zeolites showing the framework built of sodalite and d6r cages. T-atoms (Si and Al) are at the junctions of the mesh. Oxygen atoms and extra-framework cations are not shown. **(b)** Auger spectra of the silver species in the cation-exchanged zeolites recorded by XPS. Multiple spectra (steps in X-ray dose of 31.5 kJ/m^2) were recorded in the same location on the sample and successive spectra show an increase in the metallic silver signal. The first recorded spectrum is marked in blue and the last recorded spectrum in red. **(c)** Modified Auger parameter plotted for the ion-exchanged FAUX[Ag$_{11}$] zeolite as a function of X-ray dose. A clear jump to the metallic value of ~726.0 eV is observed after a critical X-ray dose of 235 ± 15 kJ/m^2. **(d)** The critical X-ray dose before the metallic form of silver dominates the Auger spectrum plotted for the zeolites used in this study.

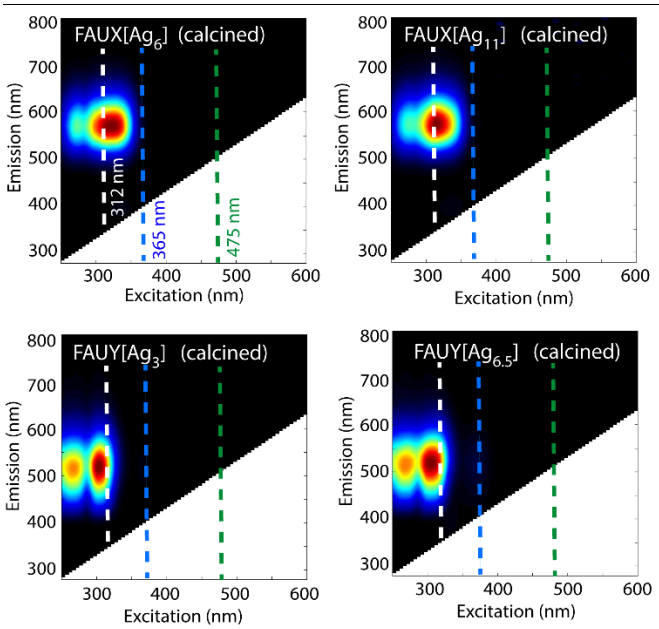

Figure 2. Two-dimensional excitation-emission plots of the four calcined zeolites studied: FAUX[Ag_6], FAUX[Ag_{11}], FAUY[Ag_3] and FAUY[$Ag_{6.5}$]. Vertical lines indicate the wavelengths used for excitation in subsequent fluorescence microscopy experiments (312 nm white, 365 nm blue, 475 nm green).

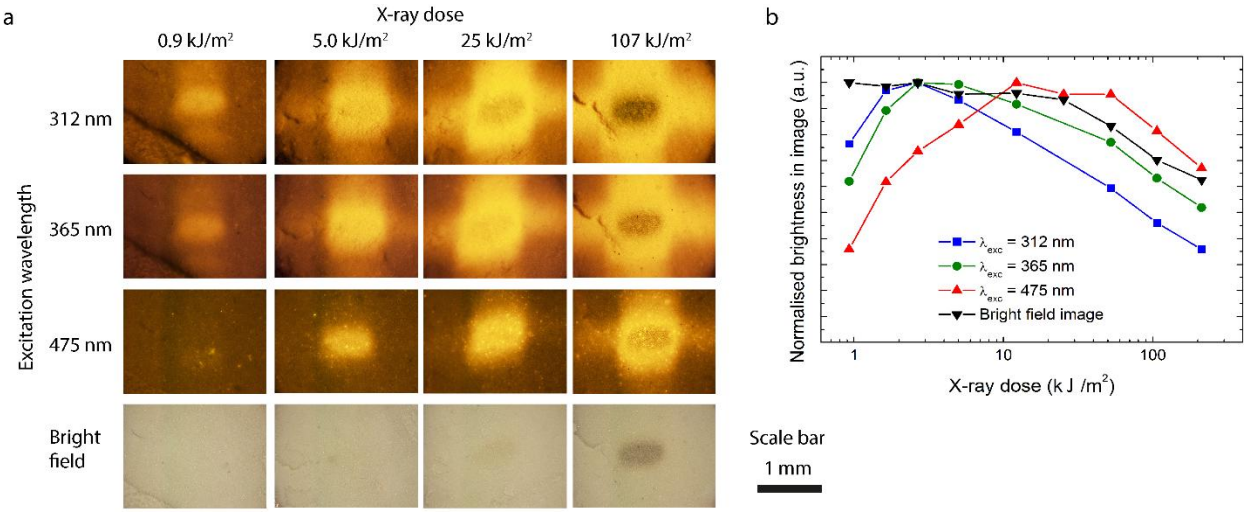

Figure 3. a Optical microscope images (2.2 mm x 1.7 mm) obtained of silver-exchanged FAUX[Ag_{11}] zeolites in powder form as a function of their X-ray exposure (dose increases from left to right). Rows from top to bottom then fluorescence images with excitation wavelengths of 312 nm, 365 nm and 475 nm, then bright field images. The full set of images is available in the supporting information. **b** Brightness of the material in the area exposed to X-rays as a function of X-ray dose. Data are normalized to the initial brightness.

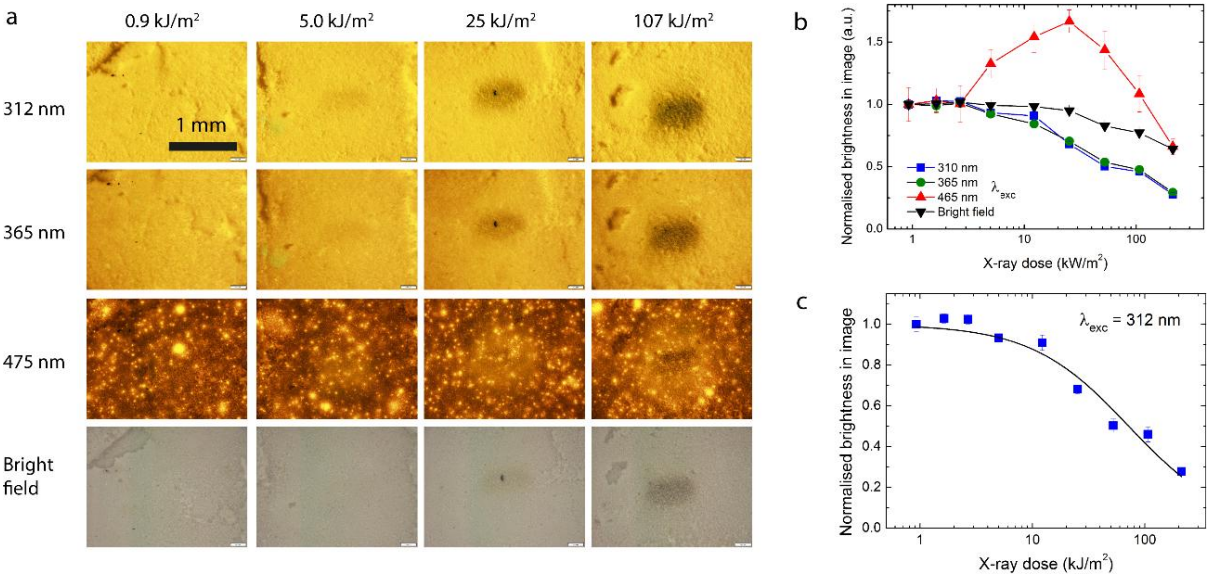

Figure 4. (a) Optical microscope images (2.2 mm x 1.7 mm) obtained of calcined FAUX[Ag_{11}] zeolites as a function of their X-ray exposure (dose increases from left to right). Rows from top to bottom then fluorescence images with excitation wavelengths of 312 nm, 365 nm and 475 nm, then bright field images. The full set of images is available in the supporting information. **(b)** Brightness of the material in the area exposed to X-rays as a function of X-ray dose. Data are normalized to the initial brightness. **(c)** Sample fitting of data from **(b)** with Equation 2.

Table 1. Stability of isolated silver atoms and clusters in the zeolites studied.

Zeolite topology	X-ray dose above which metallic signal dominates the Auger spectrum	
	Low silver loading	High silver loading
FAUX	[Ag_6] 80 ± 15 kJ/m^2	[Ag_{11}] 235 ± 15 kJ/m^2
FAUY	[Ag_3] 25 ± 8 kJ/m^2	[$Ag_{6.5}$] 41 ± 9 kJ/m^2

Luminescent silver clusters can be formed in zeolite frameworks by X-ray irradiation, but they have a broader size distribution. Cluster growth dynamics is framework dependent and is also dependent on degree of silver loading in the framework. Growth from cations to luminescent clusters then non-luminescent metallic nanoparticles is observed.

O. Fenwick,* E. Coutiño-Gonzalez,* F. Richard, S. Bonacchi, W. Baekelant, D. de Vos,

M. B. J. Roeffaers, J. Hofkens,* and P. Samorì*

X-ray induced growth dynamics of luminescent silver clusters in zeolites

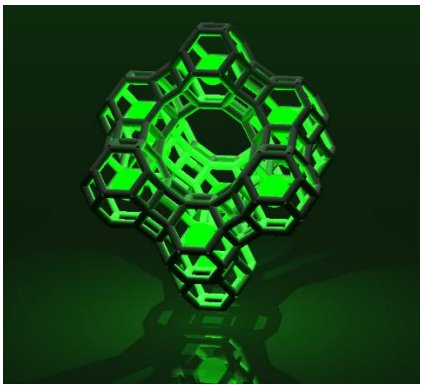

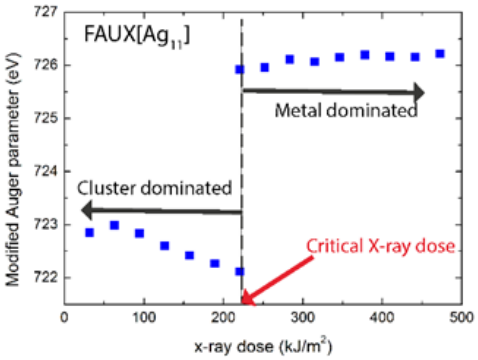

Supporting Information

X-ray induced growth dynamics of luminescent silver clusters in zeolites

Oliver Fenwick, Eduardo Coutiño-Gonzalez,* Fanny Richard, Sara Bonacchi, Wouter Baekelant, Dirk de Vos, Maarten B.J. Roeffaers, Johan Hofkens,* and Paolo Samorì.**

1. **Optical images**

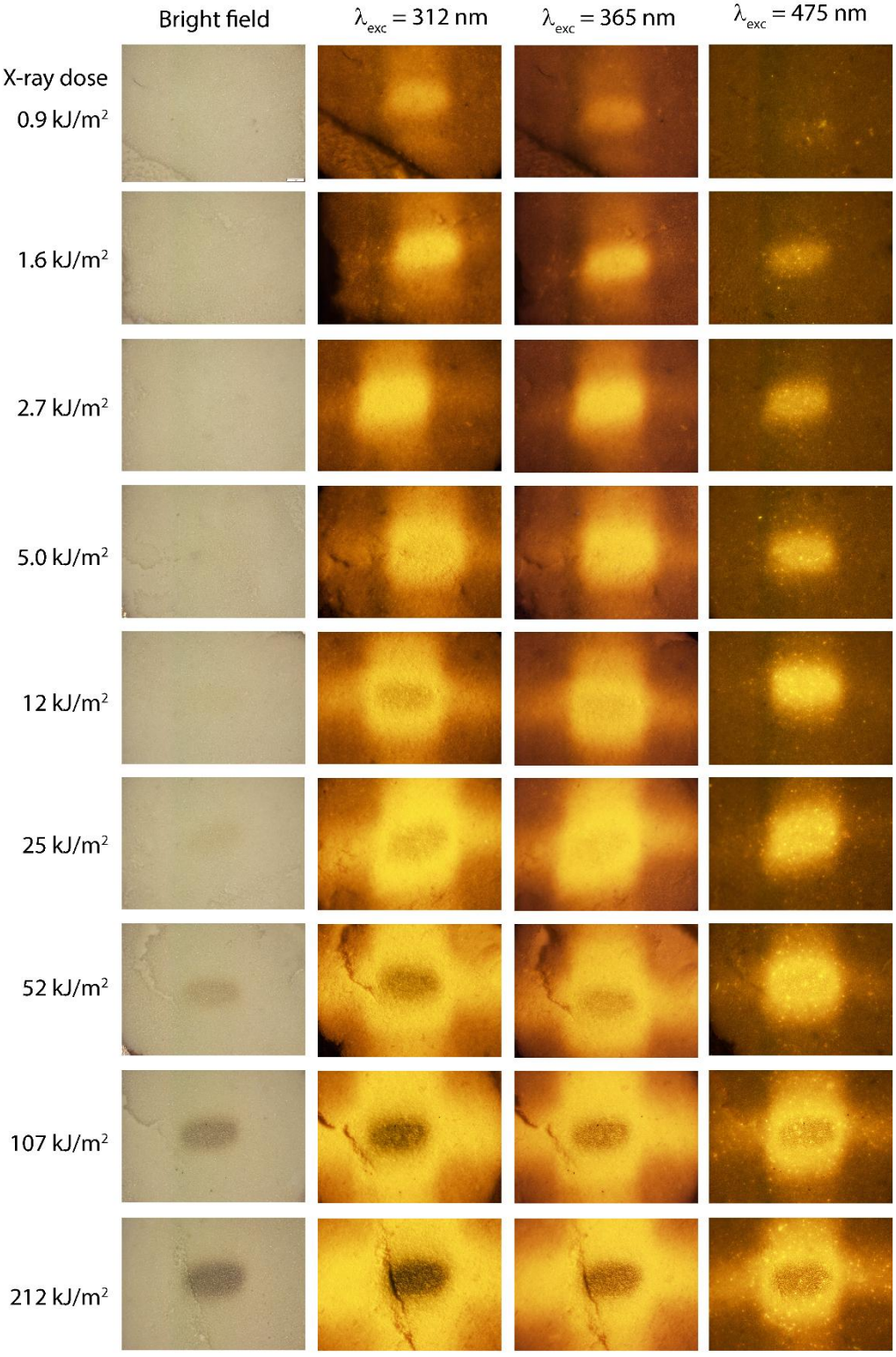

Figure S1 – Optical microscope images (2.2 mm x 1.7 mm) obtained of dry silver-exchanged FAUX[Ag_{11}] zeolites as a function of their X-ray exposure (dose increases as you move down the column). Columns from left to right contain bright field images, then fluorescence images with excitation wavelengths of 312 nm, 365 nm then 475 nm.

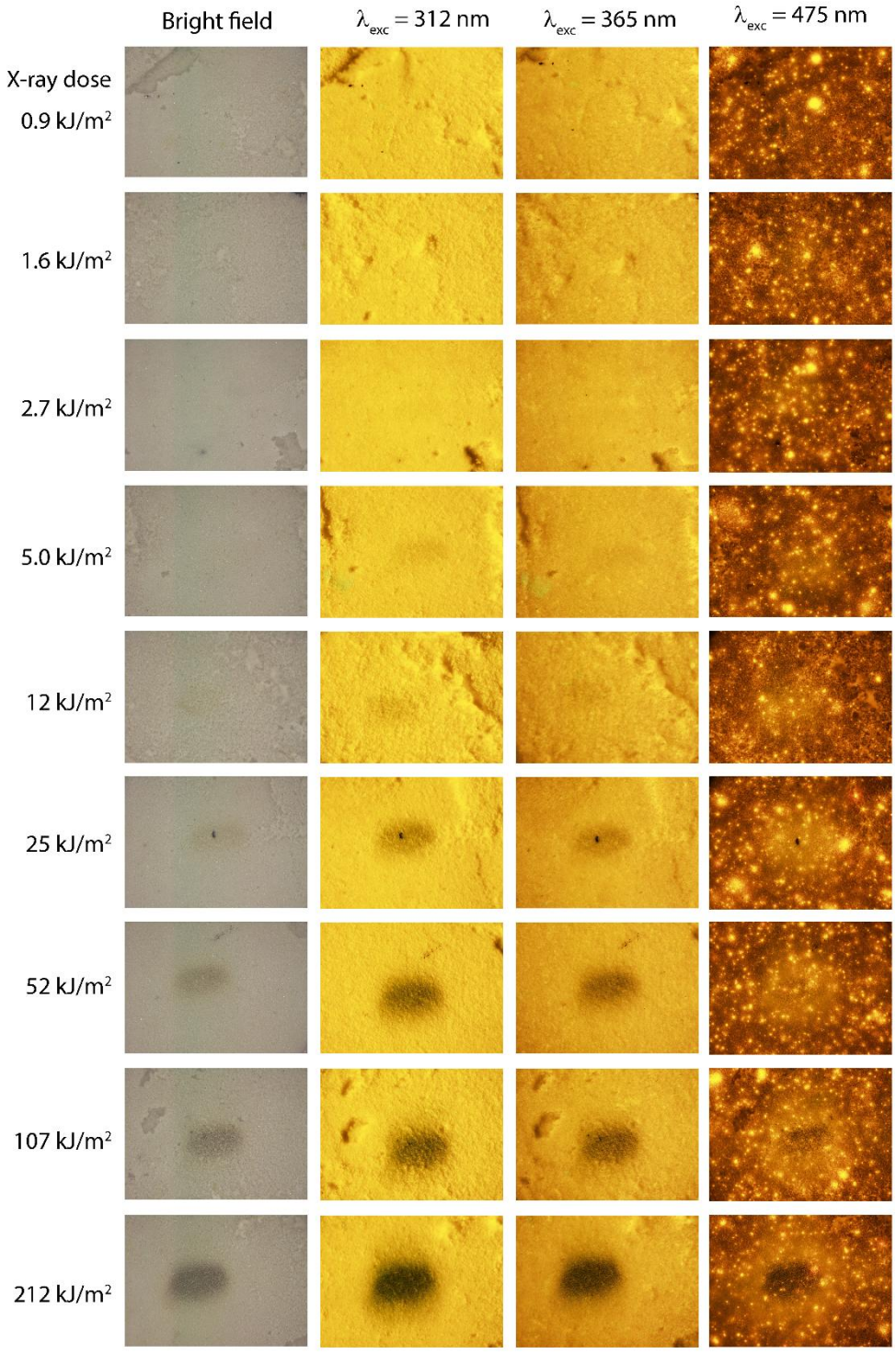

Figure S2 – Optical microscope images (2.2 mm x 1.7 mm) obtained of silver-exchanged and calcined FAUX[Ag_{11}] zeolites as a function of their X-ray exposure (dose increases as you move down the column). Columns from left to right contain bright field images, then fluorescence images with excitation wavelengths of 312 nm, 365 nm then 475 nm.

2. XPS data.

Table S1 – Binding energies of Ag $3d^5$ electrons and kinetic energies of the Ag $M_4N_{4,5}N_{4,5}$ electrons of FAUX[Ag_6] as a function of X-ray dose (hν = 1486.7 eV, 66 Wm^{-2}). The modified Auger parameters shown in the final column are derived from the sum of the binding energy of Ag $3d^5$ electrons and kinetic energy of the Ag $M_4N_{4,5}N_{4,5}$ electrons.

Dose (kJ/m^2)	Ag $3d^5$ binding energy (eV)	Auger $M_4N_{4,5}N_{4,5}$ electron kinetic energy (eV)	Modified Auger parameter (eV)
8.3	369.9	352.5	722.4
15.8	369.4	353.2	722.6
24.9	371.0	352.8	723.8
41.5	370.9	352.7	723.6
47.3	370.1	353.0	723.1
58.1	370.9	352.5	723.4
78.8	370.1	355.6	725.7
91.3	370.7	355.4	726.1
107.9	370.6	355.7	726.3
110.3	370.1	355.9	726.0
141.9	370.0	356.1	726.1
173.4	370.0	356.3	726.3
204.9	369.9	356.3	726.2
236.4	369.9	356.4	726.3
267.9	369.9	356.3	726.2
299.5	369.8	356.5	726.3
331.0	369.8	356.6	726.4
362.5	369.8	356.6	726.4
394.0	369.8	356.6	726.4
425.5	369.7	356.6	726.3
457.1	369.7	356.6	726.3
0 [calcined]	368.2	353.9	722.1

Table S2 – Binding energies of Ag $3d^5$ electrons and kinetic energies of the Ag $M_4N_{4,5}N_{4,5}$ electrons of FAUX[Ag_{11}] as a function of X-ray dose (hν = 1486.7 eV, 66 Wm^{-2}). The modified Auger parameters shown in the final column are derived from the sum of the binding energy of Ag $3d^5$ electrons and kinetic energy of the Ag $M_4N_{4,5}N_{4,5}$ electrons.

Dose (kJ/m^2)	Ag $3d^5$ binding energy (eV)	Auger $M_4N_{4,5}N_{4,5}$ electron kinetic energy (eV)	Modified Auger parameter (eV)
31.5	370.0	352.9	722.9
63	370.2	352.8	723.0
94.5	370.1	352.7	722.8
126	370.0	352.6	722.6
157.5	369.9	352.5	722.4
189	369.9	352.4	722.3
220.5	369.8	352.3	722.1
220.5	369.8	356.1	725.9
252	369.8	356.2	726.0
283.5	369.7	356.4	726.1
315	369.7	356.4	726.1
346.5	369.7	356.5	726.2
378	369.6	356.6	726.2
409.5	369.6	356.6	726.2
441	369.6	356.6	726.2
472.5	369.5	356.7	726.2
0 [calcined]	368.3	353.9	722.2

Table S3 – Binding energies of Ag $3d^5$ electrons and kinetic energies of the Ag $M_4N_{4,5}N_{4,5}$ electrons of FAUY[Ag_3] as a function of X-ray dose ($h\nu$ = 1486.7 eV, 66 Wm^{-2}). The modified Auger parameters shown in the final column are derived from the sum of the binding energy of Ag $3d^5$ electrons and kinetic energy of the Ag $M_4N_{4,5}N_{4,5}$ electrons.

Dose (kJ/m^2)	Ag $3d^5$ binding energy (eV)	Auger $M_4N_{4,5}N_{4,5}$ electron kinetic energy (eV)	Modified Auger parameter (eV)
8.3	370.4	352.1	722.5
8.3	370.4	354.7	725.1
15.8	369.7	355.3	725.0
24.9	370.5	355.0	725.5
41.5	370.3	355.4	725.7
47.3	369.8	355.6	725.4
58.1	370.1	355.6	725.7
74.7	370.0	355.7	725.7
78.8	369.7	355.8	725.5
91.3	370.0	355.8	725.8
107.9	369.9	356.0	725.9
110.3	369.7	355.7	725.4
141.8	369.7	355.8	725.5
173.3	369.7	355.9	725.6
204.8	369.6	355.9	725.5
236.3	369.6	355.9	725.5
267.8	369.6	356.0	725.6
299.3	369.6	355.9	725.5
330.8	369.5	355.8	725.3
362.3	369.5	355.9	725.4
393.8	369.5	355.9	725.4
425.3	369.5	355.9	725.4
456.8	369.5	356.0	725.5

Table S4 – Binding energies of Ag $3d^5$ electrons and kinetic energies of the Ag $M_4N_{4,5}N_{4,5}$ electrons of FAUY[$Ag_{6.5}$] as a function of X-ray dose (hν = 1486.7 eV, 66 Wm^{-2}). The modified Auger parameters shown in the final column are derived from the sum of the binding energy of Ag $3d^5$ electrons and kinetic energy of the Ag $M_4N_{4,5}N_{4,5}$ electrons.

Dose (kJ/m^2)	Ag $3d^5$ binding energy (eV)	Auger $M_4N_{4,5}N_{4,5}$ electron kinetic energy (eV)	Modified Auger parameter (eV)
8.3	370.0	352.0	721.96
15.8	370.3	351.8	722.1
24.9	370.6	351.2	721.76
24.9	370.6	354.2	724.76
41.5	370.6	354.7	725.34
47.3	370.5	354.8	725.3
58.1	370.7	354.7	725.36
74.7	370.7	354.8	725.46
78.8	370.3	355.1	725.4
91.3	370.7	355.0	725.67
107.9	370.6	355.0	725.59
110.3	370.2	355.2	725.4
141.8	370.2	355.4	725.6
173.3	370.1	355.4	725.5
204.8	370.1	355.6	725.7
236.3	370.2	355.6	725.7
267.8	370.0	355.6	725.6
299.3	370.0	355.6	725.6
330.8	370.0	355.6	725.6
362.3	370.0	355.7	725.7
393.8	369.9	355.7	725.6
425.3	369.9	355.8	725.7
456.8	369.9	355.8	725.7
0 [calcined]	368.63	353.6	722.23

3. Thermogravimetric analysis.

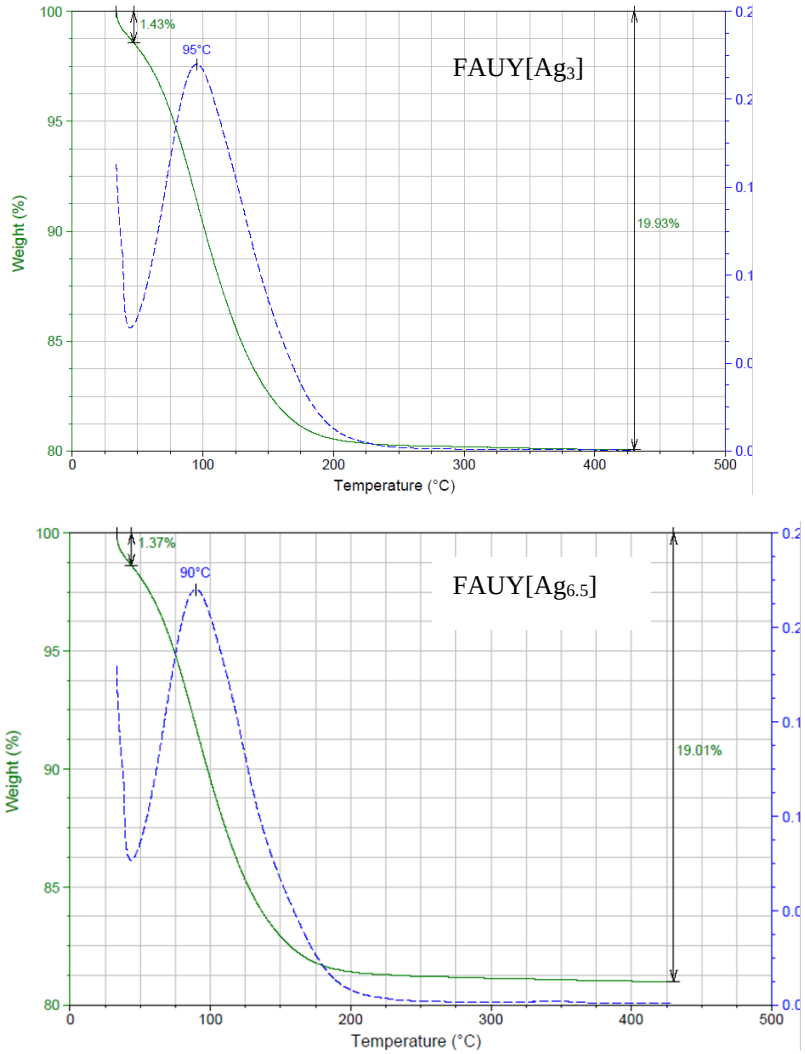

Figure S3 – Thermogravimetric analysis of our FAUY zeolites showing the onset of dehydration at ~35°C, and complete dehydration by 450°C, even under the relatively short timescale of the TGA measurement.

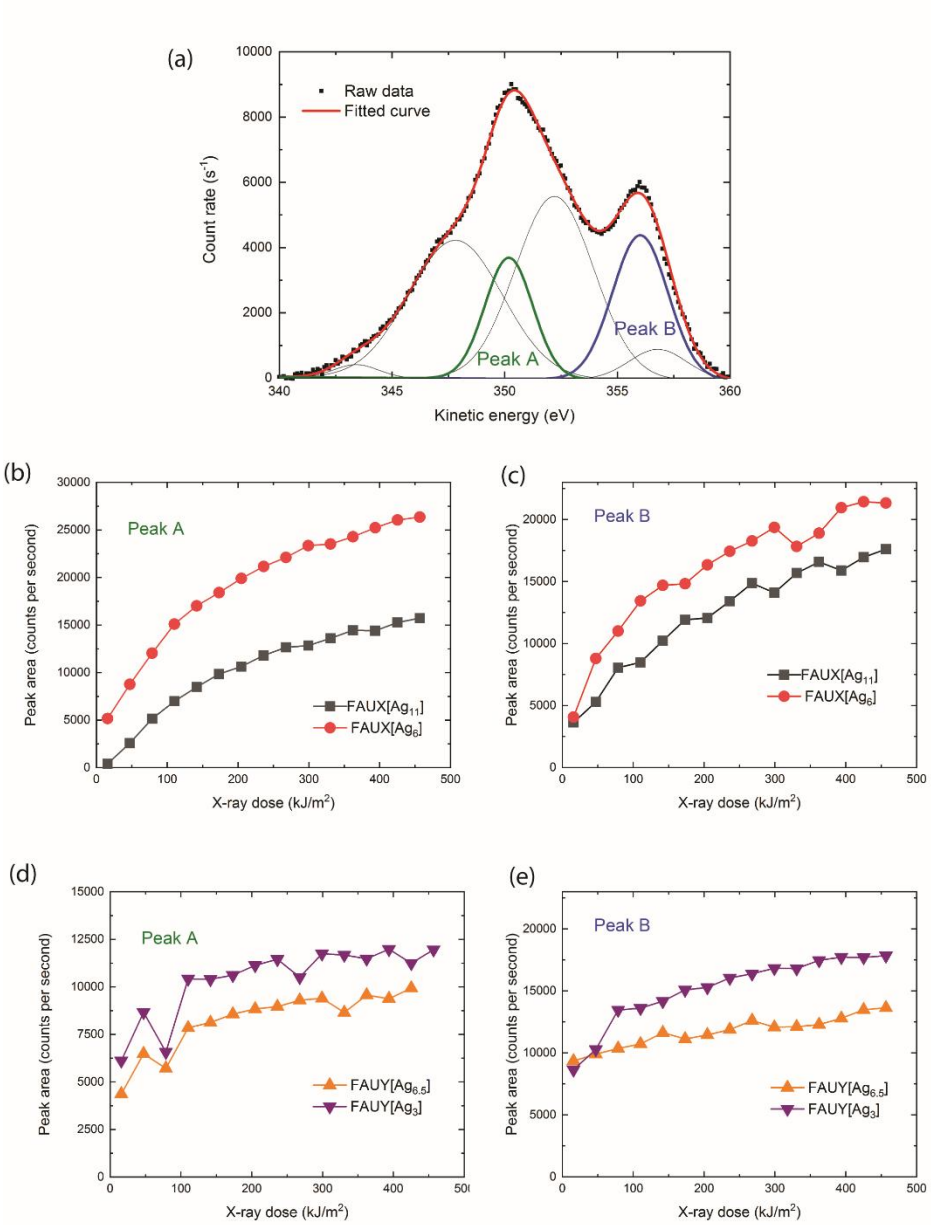

Figure S4 – Fitted peaks of Auger electron spectra evolution with X-ray dose. (a) example fitted spectrum, with two of the characteristic metallic peaks labelled. Fitted peak area plotted as a function of X-ray dose for FAUX zeolites for peak A (b) and Peak B (c). Fitted peak area plotted as a function of X-ray dose for FAUY zeolites for peak A (d) and Peak B (e).